# Occurrence of Graphite-Like Carbon in Podiform Chromitites of Greece and Its Genetic Significance

**Maria Economou-Eliopoulos \*, George Tsoupas and Vasilis Skounakis**

Department of Geology and Geoenvironment, University of Athens, Athens 15784, Greece;
gtsoupas@geol.uoa.gr (G.T.); vskoun@geol.uoa.gr (V.S.)
**\*** Correspondence: econom@geol.uoa.gr; Tel.: +30-2107274214

check for
updates

**Abstract:** The role of post-magmatic processes in the composition of chromitites hosted in ophiolite complexes, the origin of super-reduced phases, and factors controlling the carbon recycling in a supra-subduction zone environment are still unclear. The present contribution compiles the first scanning electron microscope/energy-dispersive (SEM/EDS) data on graphite-like amorphous carbon, with geochemical and mineral chemistry data, from chromitites of the Skyros, Othrys, Pindos, and Veria ophiolites (Greece). The aim of this study was the delineation of potential relationships between the modified composition of chromite and the role of redox conditions, during the long-term evolution of chromitites in a supra-subduction zone environment. Chromitites are characterized by a strong brittle (cataclastic) texture and the presence of phases indicative of super-reducing phases, such as Fe–Ni–Cr-alloys, awaruite ($Ni_3Fe$), and heazlewoodite ($Ni_3S_2$). Carbon-bearing assemblages are better revealed on Au-coated unpolished sections. Graphite occurs in association with hydrous silicates (chlorite, serpentine) and $Fe^{2+}$-chromite, as inclusions in chromite, filling cracks within chromite, or as nodule-like graphite aggregates. X-ray spectra of graphite–silicate aggregates showed the presence of C, Si, Mg, Al, O in variable proportions, and occasionally K and Ca. The extremely low $fO_2$ during serpentinization facilitated the occurrence of methane in microfractures of chromitites, the precipitation of super-reducing phases (metal alloys, awaruite, heazlewoodite), and graphite. In addition, although the origin of Fe–Cu–Ni-sulfides in ultramafic parts of ophiolite complexes is still unclear, in the case of the Othrys chromitites, potential reduction-induced sulfide and/or carbon saturation may drive formation of sulfide ores and graphite-bearing chromitites. The presented data on chromitites covering a wide range in platinum-group element (PGE) content, from less than 100 ppb in the Othrys to 25 ppm ΣPGE in the Veria ores, showed similarity in the abundance of graphite-like carbon. The lack of any relationship between graphite (and probably methane) and the PGE content may be related to the occurrence of the (Ru–Os–Ir) minerals in chromitites, which occur mostly as oxides/hydroxides, and to lesser amounts of laurite, with pure Ru instead activating the stable $CO_2$ molecule and reducing it to methane (experimental data from literature).

**Keywords:** graphite; chromitite; ophiolite; metal alloys; super-reducing conditions; Greece

## 1. Introduction

The origin of chromite deposits and occurrences in a hydrous supra-subduction zone (SSZ) environment is a common feature for major ophiolite complexes [1–11]. However, the origin of minerals indicative of super-reducing (SuR), ultra-high-pressure (UHP) conditions (diamonds, coesite, stishovite, moissanite, native elements, and alloys), and subducted material (quartz, zircon, corundum) incorporated into chromitites is a topic of debate [10–18]. It was suggested that the presence of such minerals in chromitites and ultramafic rocks is associated with potential recycling into the ultra-deep mantle by continued subduction [15–17], whereas others suggested that post-magmatic

processes, during an extended period of the ductile asthenospheric mantle flow to shallow crustal brittle deformation, may modify the primary magmatic compositional trends in chromitites and rocks [11–18].

The serpentinization process is potentially important, involving the transfer of large amounts of fluid, and strongly influences oxidation equilibria, and examined in detail for ultramafic systems [19]. Recently, the discovery of abiotic $CH_4$ generated from serpentinized peridotites and chromitites associated with ophiolite complexes led to an increasing number of case studies from worldwide localities in which $CH_4$ was reported [20–24]. Methane ($CH_4$) can be produced via Fischer–Tropsch-type reactions (like the Sabatier reaction) between $CO_2$ (or other C compounds) and $H_2$ (from serpentinization) at low temperatures (typically <100 °C) [22,24,25]. The abiotic methanogenesis in ultramafic rocks is well documented at shallow conditions, whilst evidence at depth (~40 km) is limited [23,24]. The role of volatiles for the association of graphite with sulfides, platinum-group element minerals (PGMs), and hydrosilicates was well established in the ultrabasic complexes of Bushveld and Stillwater [13,26–28]. Late-magmatic C–O–H–S fluids are considered as responsible for such mineral assemblages [13]. In the Othrys and Vourinos ophiolite complexes of Greece, methane was described in microfractures and porous serpentine- or chlorite-filled veins [22].

In our contribution, we present the first SEM/EDS data from polished and unpolished sections on graphite-like amorphous carbon (the term graphite is used in the text) associated with serpentine and/or chlorite inclusions within chromite grains, along fractures, and as interstitial in selected samples of chromitites of the Skyros, Othrys, Pindos, and Veria ophiolites, with variable platinum-group element (PGE; Os, Ir, Ru, Pt, and Pd) content, aiming at delineating potential relationships with modified composition in the associated chromite, as well as the role of redox conditions and Ru (PGE), during the long-term evolution of chromitites in a supra-subduction zone environment.

## 2. Materials and Methods

Polished and unpolished thick sections of chromitites from the Skyros, Othrys, Pindos, and Veria (Greece) chromite occurrences and deposits were prepared. Special attention was paid to the SEM examination of chromitites, because a potential contamination by carbon is a well-known problem, involving the preparation of polished sections, the SEM/EDS analysis, sublimation of carbon coatings from previous samples in the high-vacuum conditions of the chamber, leakages from the pumping system, and outgassing of other internal SEM parts [18,29,30]. Unpolished sections are small fragments (samples cut using a hammer or using corundum ($Al_2O_3$) that is carbon free), which were used in order to avoid contamination by the polishing material. A diamond abrasive paste of 1-μm particle size was used for polishing the polished sections, and an ultrasonic bath was used to remove any remaining polishing material from the samples. The polished sections for the SEM/EDS analysis were Au-coated in a chamber used for the sublimation of Au coatings only, in order to avoid contamination by carbon from previous samples in the high-vacuum conditions of the chamber sublimation. A synthetic sample of graphene oxide was used (Figure 1), in order to arrange accelerating voltage up to 8 kV, having a very clear C peak in spectra from chromitite thick sections. All studied samples were examined at the University of Athens (Department of Geology and Geoenvironment) and the National and Kapodistrian University of Athens (NKUA), initially by reflected light microscopy and a JEOL JSM 5600 scanning electron microscope (SEM) (JEOL, Tokyo, Japan), equipped with the ISIS 300 OXFORD automated energy-dispersive X-ray instrument, with the following operating conditions: accelerating voltage, 20 kV; beam current, 0.5 nA; time of measurement (dead time), 50 s; and beam diameter, 1–2 μm. The following X-ray lines were used: OsMα, PtMα, IrMα, AuMα, AgLα, AsLα, FeKα, NiKα, CoKα, CuKα, CrKα, AlKα, TiKα, CaKα, SiKα, MnKα, MgKα, and ClKα. Standards used were pure metals for the elements Os, Ir, Ru, Rh, Pt, Pd, Cu, Ni, Co, and Cr, while indium arsenide was used for As and pyrite was used for S and Fe.
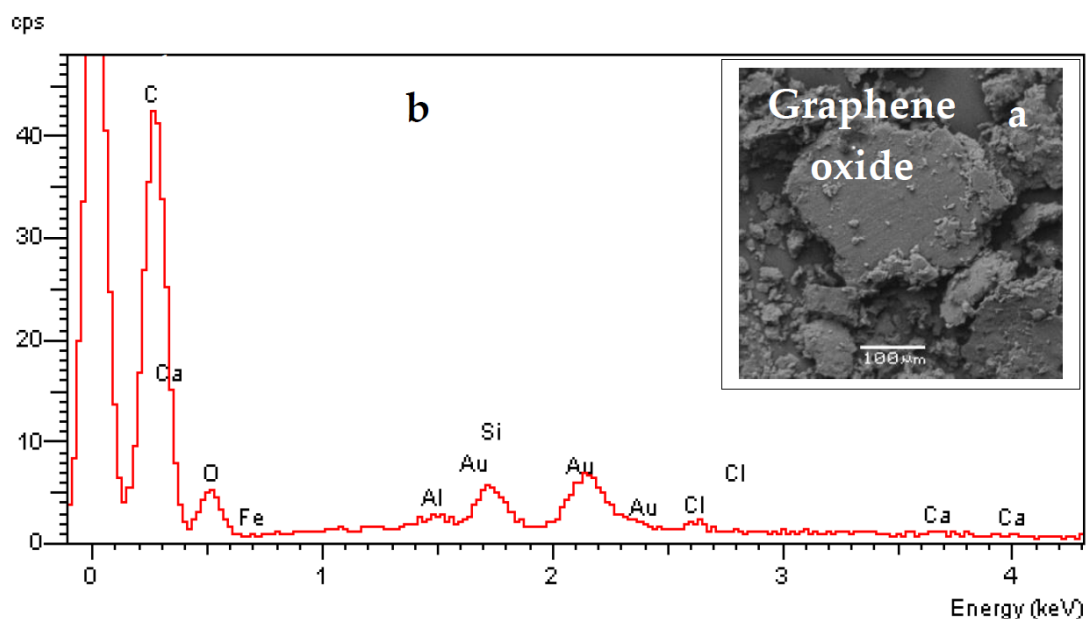
**Figure 1.** Back-scattered electron image (Au-coating of unpolished section) of synthetic graphene oxide (**a**), and corresponding X-ray spectra (**b**).

Major and trace elements in massive chromitite samples were determined by Inductively Coupled Plasma Mass Spectrometry (ICP-MS) analysis, at Bureau Veritas Labs, formerly ACME Laboratories Ltd., Vancouver, BC, Canada. The samples were dissolved using a strong multi-acid ($HNO_3$–$HClO_4$–HF) digestion, and the residues were dissolved in concentrated HCl. Platinum-group element (PGE) analyses were carried out using Ni-sulfide fire-assay pre-concentration technique, with the nickel fire-assay technique from large (30 g) samples. This method allows for complete dissolution of samples. Detection limits were 5 ppb for Ru, 2 ppb for Os, Ir, Pt, and Pd, and 1 ppb for Rh and Au. CDN-PGMS-23 was used as standard.

## 3. Characteristics of Ophiolites and Chromitites

### 3.1. Characteristics of Ophiolites

The ophiolites of Greece have a north-northwest–south-southeast (NNW–SSE) strike, and outcrop in a discontinuous and narrow belt to the west of the Pelagonian Massif [5–7,29]. They are a significant component of the Upper Jurassic to Lower Cretaceous Tethyan ophiolite belt, which extends through Albania to the Pindos and Othrys complexes in the south (Subpelagonian zone, Figure 2) and to the Serbian zone of the Dinarides in the north [31]. These ophiolites are characterized by petrological and geochemical features which show strong similarities with ophiolites formed in a fore-arc or back-arc marginal basin in a supra-subduction zone (SSZ) environment [1,5–7,32]. Additionally, structural and paleomagnetic studies on those ophiolites revealed widespread heterogeneous deformation and rotation during their original displacement and subsequent tectonic incorporation into continental margins [7].
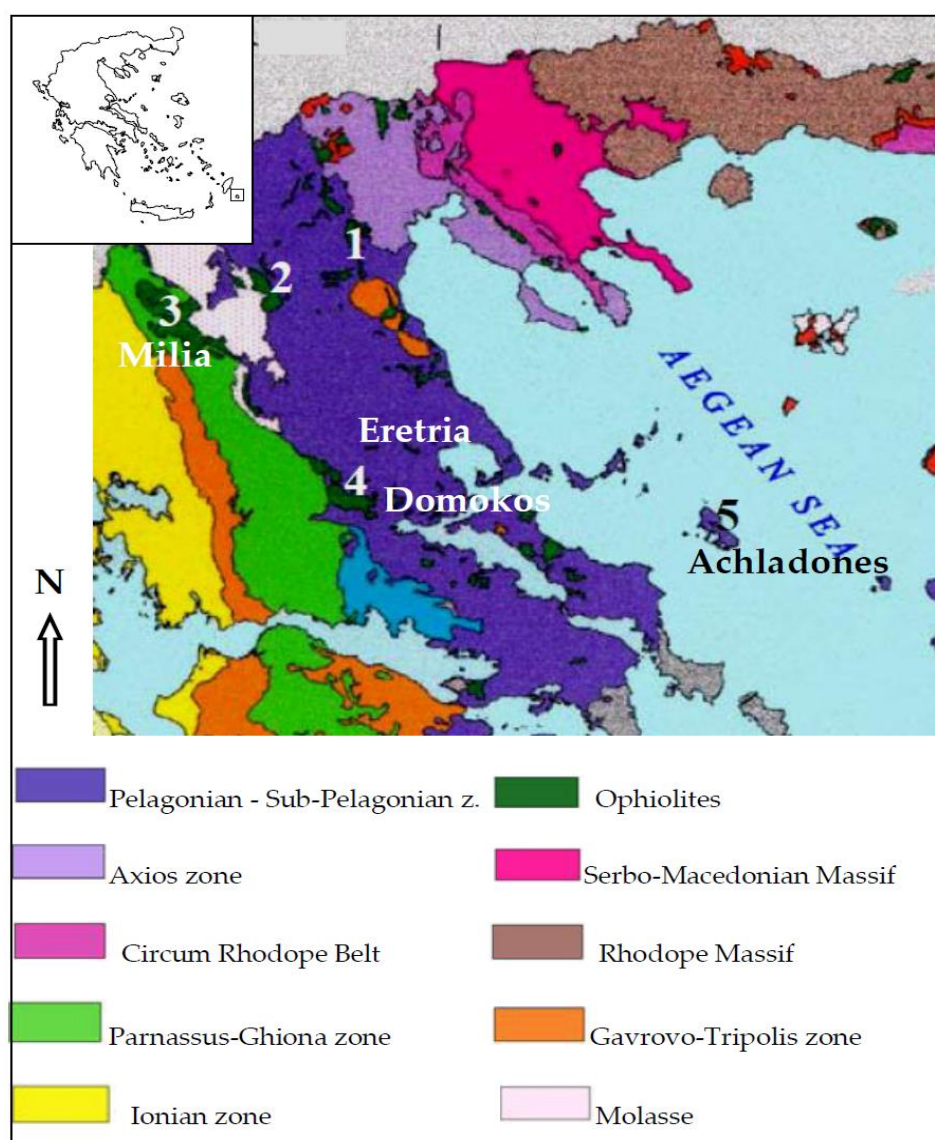
**Figure 2.** Sketch map of Hellenides [33], showing the ophiolite complexes from which chromitite samples were studied. Ophiolites: 1 = Veria; 2 = Vourinos; 3 = Pindos; 4 = Othrys; 5 = Skyros island.

## 3.2. Characteristics of Graphite-Bearing Chromitites

### 3.2.1. Skyros (Achladones)

Relatively small isolated ophiolite masses, of mostly serpentinized dunite and harzburgite, are located at the western margin of the Axios zone (Vermio–Veria), and the Eohellenic Pre-Cretaceous nape, including the Skyros island (Figure 2). At the Achladones area on the Skyros island, small massive chromitite bodies of high-Al type, with an average Cr# (Cr/(Cr + Al)) ratio of 0.56 and an Mg# (Mg/(Mg + $Fe^{2+}$)) ratio of 0.64, contain elevated PGE contents, up to 3 ppm ΣPGE, although both high-Cr and high-Al types are found across the entire island [1].

Laurite occurs as (a) single inclusions in chromite, with variable Ir and Os contents [22], and (b) Ru-, Ir-, and Os-sulfides and alloys found as interstitial to strongly fragmented chromite grains, having significant Ni, Cr, Fe As, and Sb contents [34]. Pyrrhotite having up to 0.5 wt. % Ni, chalcopyrite with traces of Ni, and pentlandite occur as small inclusions in chromite, heazlewoodite ($Ni_3S_2$), and millerite (NiS) in the serpentinized matrix and in cracks penetrating chromite grains, while elongated crystals of graphite are the most abundant inclusions in magnetite ore [35].

### 3.2.2. Othrys (Eretria)

The Othrys ophiolite complex includes two tectonically separated chromite deposits, namely Eretria (Tsagli) and Domokos (Figure 2). The combined tonnage together with several other occurrences, including the Agios Stefanos, involves approximately 3 Mt of high-Al massive chromite ores, with a Cr# ratio ranging from 0.53 to 0.62, hosted in moderated depleted harzburgite, while containing low PGE contents, mostly less than one hundred ΣPGE [1,32,34]. Zircons occur as inclusions in Cr-spinel and are commonly cross-cut by fractures and show evidence for pseudomorphic replacement by Ca-rich zircon silicates, due probably to re-equilibration with secondary fluids [33]. The occurrence of massive Fe–Ni–Cu-sulfide mineralization (pyrrhotite, chalcopyrite, and minor Co-pentlandite) at the peripheral parts of podiform chromite bodies in association with magnetite [36], and considerable amounts of methane in microfractures and porous serpentine- or chlorite-filled veins [22,27] are salient features of the Othrys chromite deposits.

### 3.2.3. Pindos (Milia)

The chromitite occurrences in the Pindos ophiolite complex are small (a few tens of meters × a few tens of centimeters) and are of all textural types (massive, schlieren, banded, disseminated, and nodular). They are high in Cr and high in Al, often in a spatial association, hosted within completely serpentinized, weathered, and intensively deformed dunite–harzburgite blocks, due to a strong plastic and brittle deformation, which had an important influence on their present form and distribution [37]. Massive chromite pods, with an average Cr# ratio of 0.82 and an Mg# ratio of 0.40, exhibited elevated PGE content (up to 1060 ppb ΣPGE) (Table 1) [37], while other chromitite occurrences at the Milia area having Cr# ratios ranging between 0.80 and 0.84, and Mg# ratios between 0.54 and 0.72 contain relatively low (≤170 ppb) PGE content [38]. At Milia, the PGMs are predominantly Os, Ir, and Ru iridium/PGE (IPGE) alloys and sulfarsenides, rather than laurite, and are all less than 5 μm in size (usually less than 2 μm), while heazlewoodite and awaruite occur in the serpentinized matrix [36]. They are all irregular in shape and mottled, showing inhomogeneity of composition. They are mainly Os–Ir–Ru–Rh (±Ni) alloys with minor Pt, altered occasionally to oxides [38,39].

### 3.2.4. Veria

Chromitites in the area of Veria occur as small irregular bodies of varying sizes (up to 15 m in length and 1 m in thickness). They were affected by intense tectonic activity, which created faulting, folding, over thrusting, foliation, lineation of minerals, and an orientation parallel to the general northwest–southeast (NW–SE) displacement direction. Chromite is dominantly of high-Cr composition, with the Cr# ratio ranging from 0.55 to 0.84, and an average value of 0.7. Interstitial primary silicates in chromitites were replaced by secondary phases consisting of mostly Cr-andradite, Cr-chlorite, and serpentine flakes in lesser amounts. Awaruite ($Ni_3Fe$) and heazlewoodite ($Ni_3S_2$) commonly occur within fractures and the serpentine–chlorite matrix. Although they are fine-grained, heazlewoodite cores sometimes occur within awaruite, suggesting a gradual transformation of the former to the latter. Certain chromitite bodies hosted at the Veria ophiolite are characterized by the presence of extremely high PGE content (up to 25 ppm) and abundant PGE minerals within massive chromite samples located along a shear zone, attributed to multi-stage mineralization processes [40].

## 4. Results

### 4.1. Mineralogical Characteristics

Structure and mineralogical data from the microscopic and SEM/EDS investigation showed that studied chromites are characterized by a strong brittle (cataclastic) texture and the presence of highly reduced phases, such as graphite, metal alloys, awaruite, and/or heazlewoodite. The Fe–Ni–Cr alloys typically occur in cracks and/or within chromite (Figures 3–6). Chromitites from mylonitic shear zones of the Veria area are characterized by abundant Cr-garnet with a dominant

chemical composition that belongs to the andradite ($Ca_3Fe^{3+}_2Si_3O_{12}$) and uvarovite ($Ca_3Cr_2Si_3O_{12}$) solid-solution series ($And_{23-71}Uv_{25-57}$), as a matrix between chromite grains and filling cracks along chromite grain boundaries or cemented chromite (Figure 6) [40]. Graphite occurs (a) as rounded, nodule-like aggregates of graphite on unpolished parts on the sections (Figure 3b–d), and (b) as fine flakes or clusters of flakes associated with hydrous minerals (chlorite and/or serpentine) within chromite (Figures 4 and 5), along cracks and/or Fe-chromite (Figure 6c–e).
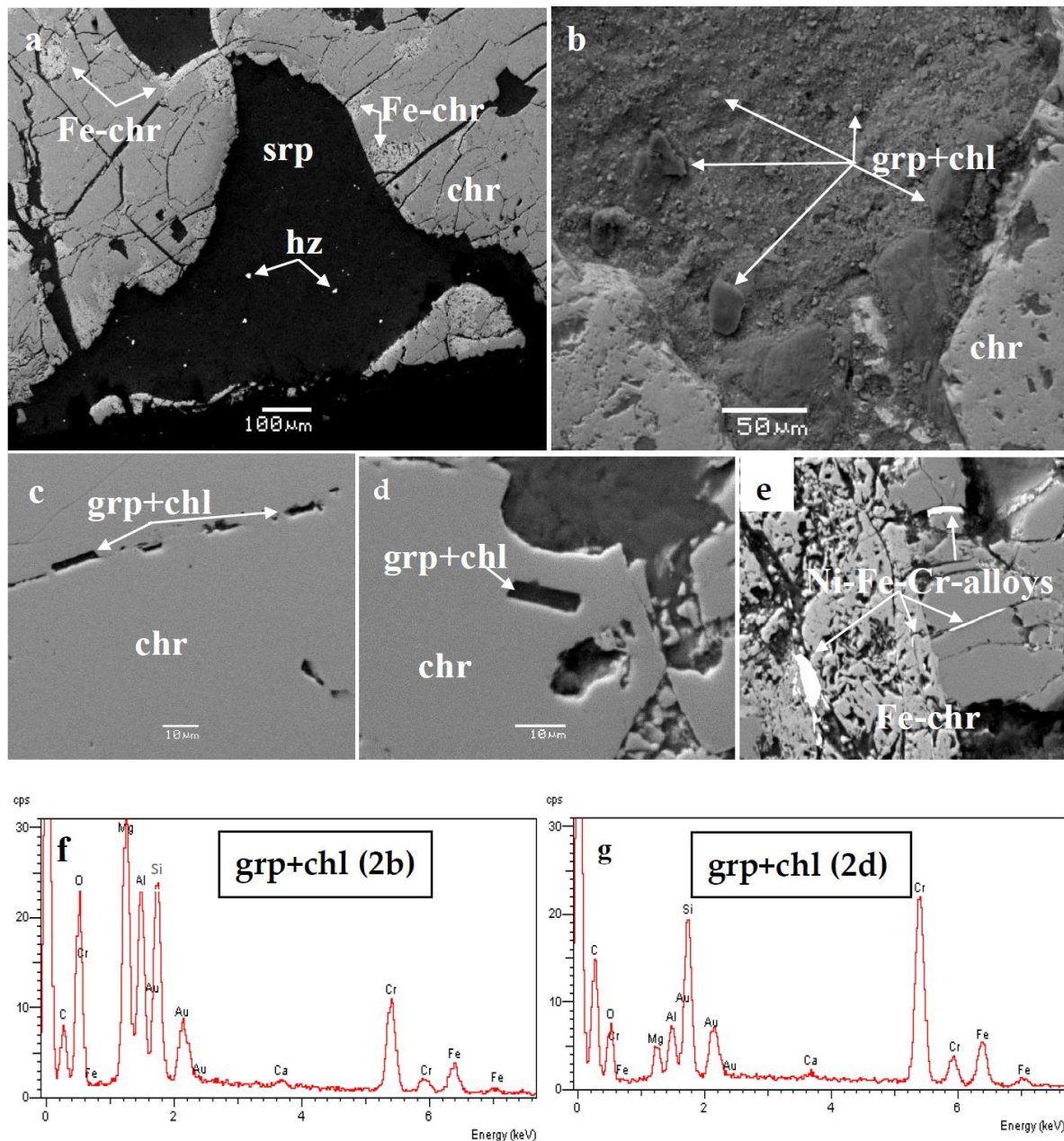


**Figure 3.** Back-scattered electron images (Au-coating of polished sections) of strongly fragmented chromitite from the Skyros ophiolite. Porous Fe-chromite is common at the peripheral parts of chromite grains (**a**). Graphite-like carbon, co-existing with silicates (chlorite), occurs as an inclusion in chromite, filling cracks within chromite, and as rounded, nodule-like aggregates. The inclusions are better revealed on unpolished parts of polished sections showing nodule-like graphite aggregates (**b–d**). Metal alloys occur within cracks cross-cutting chromite grains (**e**). X-ray spectra of graphite–silicate assemblages showed the presence of C, Si, Mg, Al, and O (**f,g**) in variable proportions. Symbols: grp = graphite; chr = chromite; Fe-chr = iron chromite; chl = chlorite; srp = serpentine; hz = heazlewoodite.
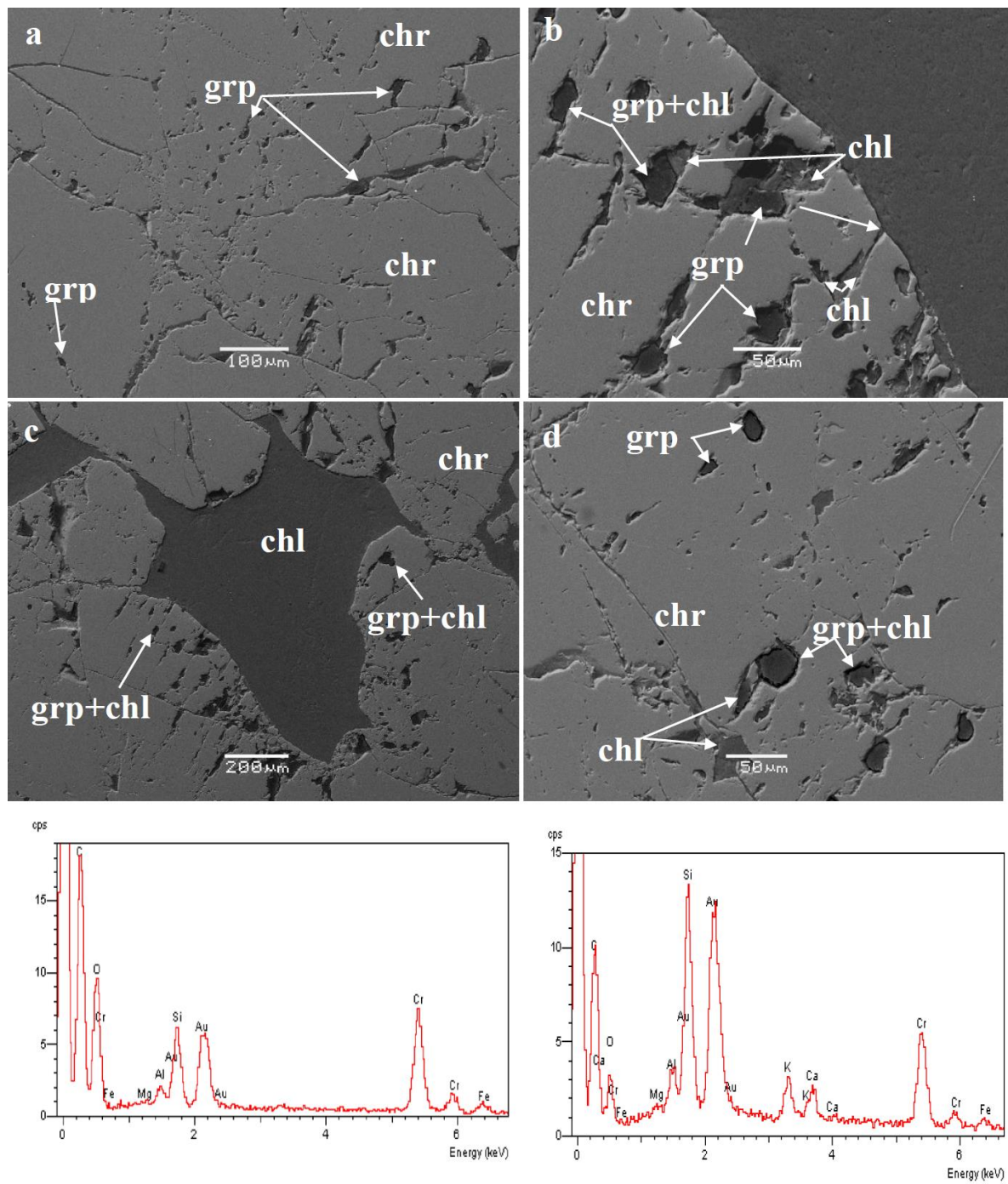
**Figure 4.** Back-scattered electron images (Au-coating of polished sections) of fragmented chromitite from the Othrys (Eretria) ophiolite complex, showing inclusion trails in chromite grains, containing graphite-like carbon, co-existing with silicates (chlorite), as well as filling cracks within chromite (**a**–**d**). X-ray spectra of graphite–silicate assemblages (**e**,**f**), chlorite (**g**), and chromite (**i**) showed the presence, in variable proportions, of C, Si, Mg, Al, O, K, and Ca. Symbols are defined in Figure 3.
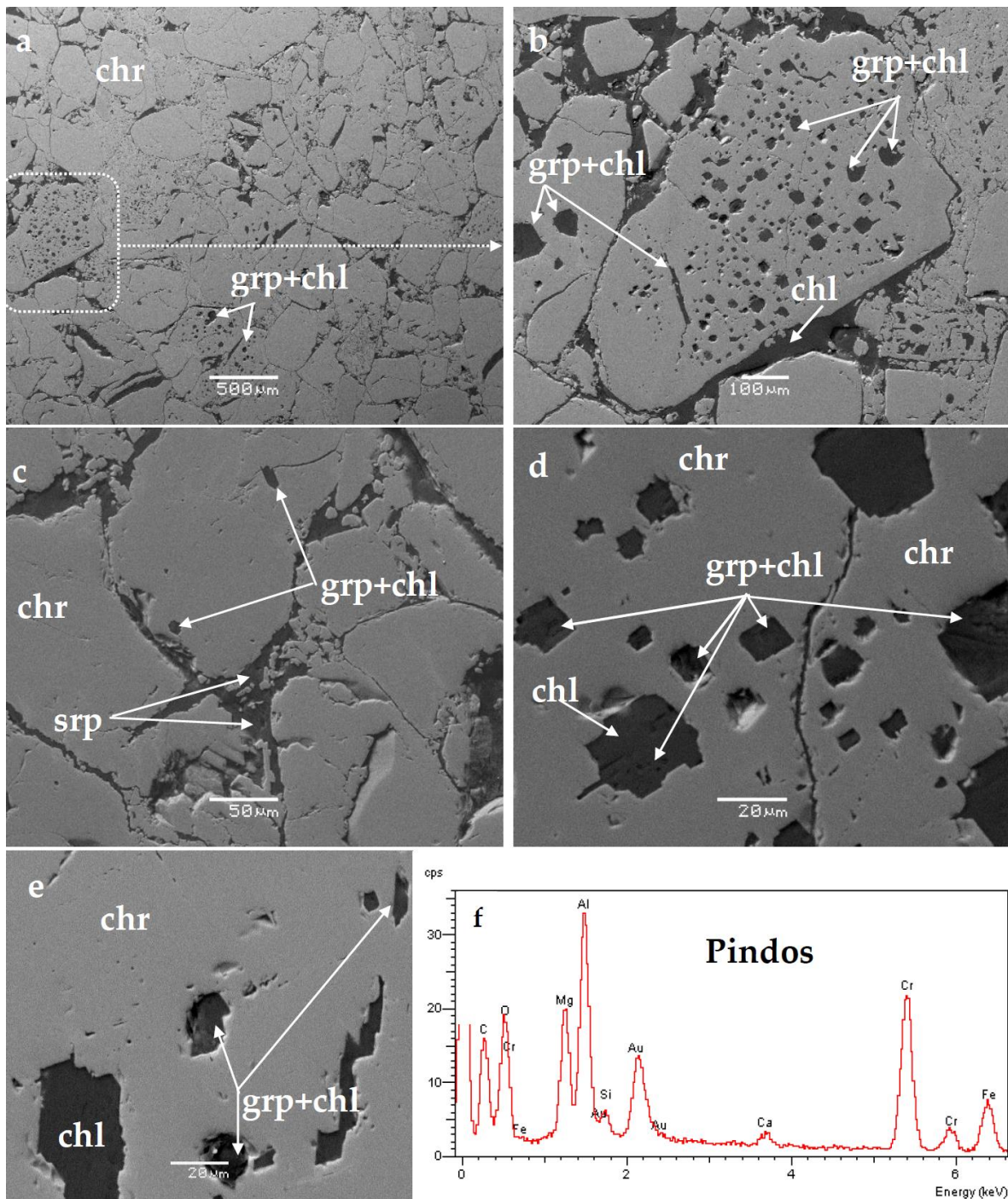
**Figure 5.** Back-scattered electron images (Au-coating of polished sections) of strongly fragmented chromitite from the Pindos (Milia) ophiolite complex, showing graphite-like carbon, co-existing with silicates, as inclusions in chromite and filling cracks within chromite (**a**–**e**, white arrows). Mold crystals with euhedral removed and/or filled by silicate–graphite aggregates are occasionally present (**d**). X-ray spectra of graphite–silicate assemblages showed the presence, in variable proportions, of C, Si, Mg, Al, and O. (**f**). Symbols are defined in Figure 3.

In the area of Veria, fragmented chromite is found either in a matrix of serpentine (Figure 6c–e) or garnet (Figure 6a,b). It appears that chromite accompanied by porous Fe-chromite was further fragmented during a subsequent event of brittle deformation (Figure 6c,d).
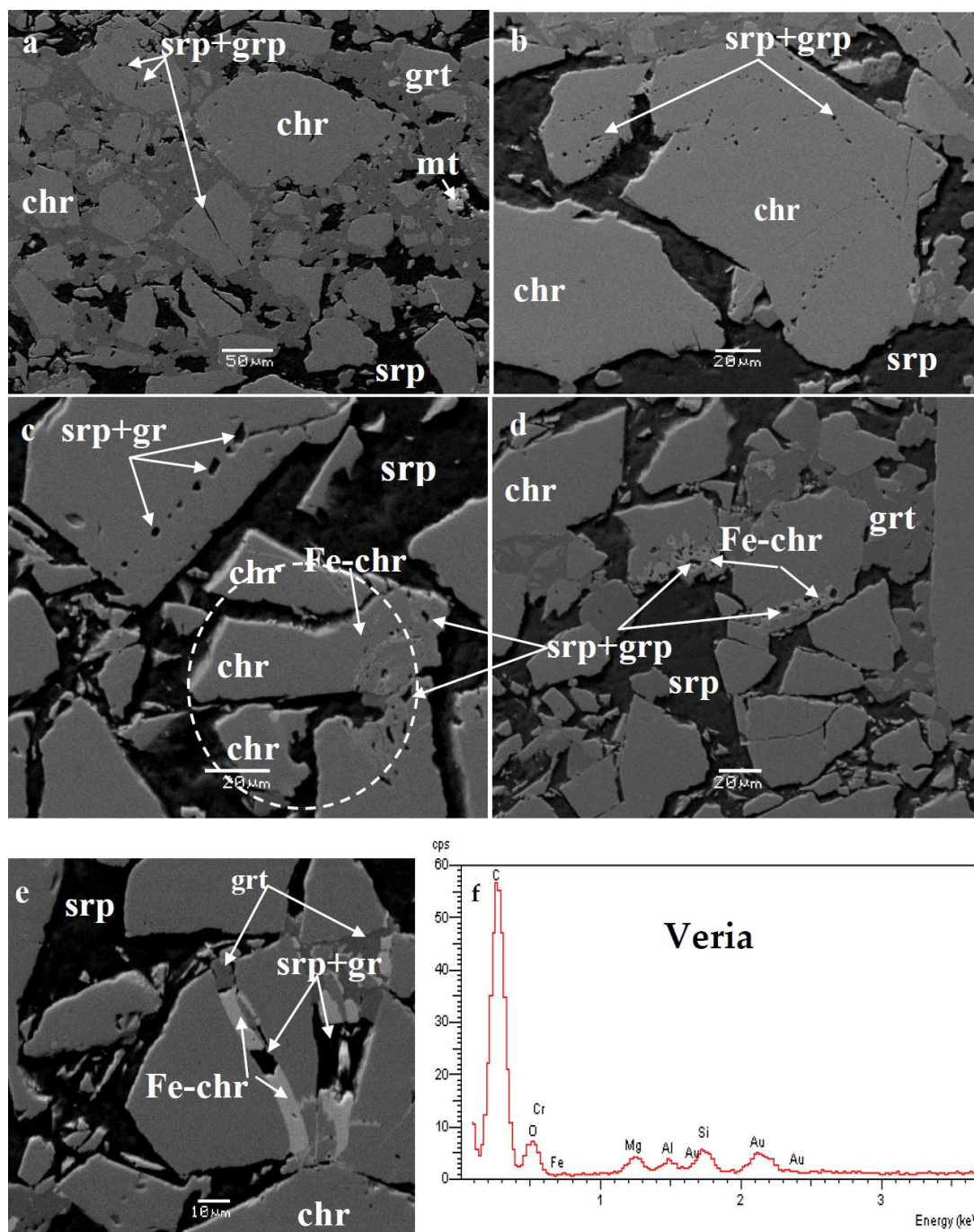
**Figure 6.** Back-scattered electron images (Au-coating of polished sections) of strongly chromitite from the Veria chromitites, showing microstructural features (**a**–**f**). Linear arrays of inclusions are common in chromite, hosted in a matrix of andradite (**a**–**c**). Serpentine flakes and graphite in a spatial association with Fe-chr (**c**–**e**). Dissolution pits in silicate inclusions of chromite are filled with graphite (**a**–**d**). Chromite fragments belonging to the same initial grain are included in the white dot cycle (**c**). The composition of Fe-chr associated with graphite (**e**) is given in Table 1. X-ray spectra of graphite–silicate assemblages showed the presence of C, Si, Mg, Al, and O (**f**). Symbols are defined in Figure 3; grt = garnet.

Representative SEM/EDS analyses of chromitites showed that unaltered core compositions fall in the field of high-Cr magnesio-chromite for the Veria and Pindos ophiolites and high-Al type for the Othrys and Skyros ores. More specifically, the magnesio-chromite composition from Pindos is of

low-ΣPGE (170 ppb) content [39], whereas the studied carbon-bearing chromitite sample from the same area (Milia) has elevated-PGE (1700 ppb) content, like the Veria sample (24 ppm PGE), and falls in the field of chromite (Tables 1 and 2). In general, the presented data show a decreasing trend of the Mg/(Mg + Fe$^{2+}$) ratio (or increase of FeO) and an increasing Cr/(Cr + Al) ratio, with the lowest value of the Mg/(Mg + Fe$^{2+}$) ratio in Fe-chromite, filling the fracture in association with graphite and silicates in the area of Veria (Figures 6d and 7; Table 1).

**Table 1.** Representative SEM/EDS analyses of magnesio-chromite and chromite from C-bearing chromitites.

| Location | Skyros | Skyros | Othrys | Othrys | Pindos | Pindos | Veria | | | | | |
|---|---|---|---|---|---|---|---|---|---|---|---|---|
| | Achladones | | Eretria | Eretria | Milia | Milia | | | | Figure 6 | | |
| wt. % | Figure 3, core | | Figure 4, core | | Figure 5, core | | Core | Core | Core | Figure 6c | Figure 6d | Figure 6e |
| Al$_2$O$_3$ | 14.5 | 19.2 | 21.4 | 22.2 | 9.6 | 8.2 | 12.8 | 12.8 | 10.3 | 4.5 | 0.6 | n.d. |
| Cr$_2$O$_3$ | 50.7 | 49.1 | 47.2 | 46.5 | 56.9 | 59.4 | 57.4 | 57.3 | 60.9 | 55.2 | 11.1 | 19.4 |
| Fe$_2$O$_3$ | 6.7 | 3.3 | 4.1 | 3.9 | 3.5 | 3.4 | 2.1 | 1.73 | 1.1 | 10.4 | 57.1 | 49.1 |
| MgO | 11.6 | 13.5 | 14.8 | 15.6 | 7.7 | 8.5 | 12.5 | 12.2 | 12.1 | 5.9 | 0.9 | n.d. |
| FeO | 16.51 | 14.2 | 12.8 | 12.6 | 21.6 | 20.2 | 14.7 | 15.1 | 15.1 | 23.4 | 29.7 | 31.3 |
| Total | 100.01 | 99.3 | 100.3 | 99.8 | 99.3 | 99.7 | 99.5 | 99.1 | 99.5 | 99.4 | 99.4 | 99.8 |
| Cr/(Cr + Al) | 0.7 | 0.63 | 0.6 | 0.58 | 0.8 | 0.82 | 0.76 | 0.75 | 0.8 | 0.89 | 0.92 | 1.00 |
| Mg/(Mg + Fe$^{2+}$) | 0.56 | 0.63 | 0.67 | 0.63 | 0.38 | 0.43 | 0.6 | 0.57 | 0.59 | 0.31 | 0.05 | 0.0 |
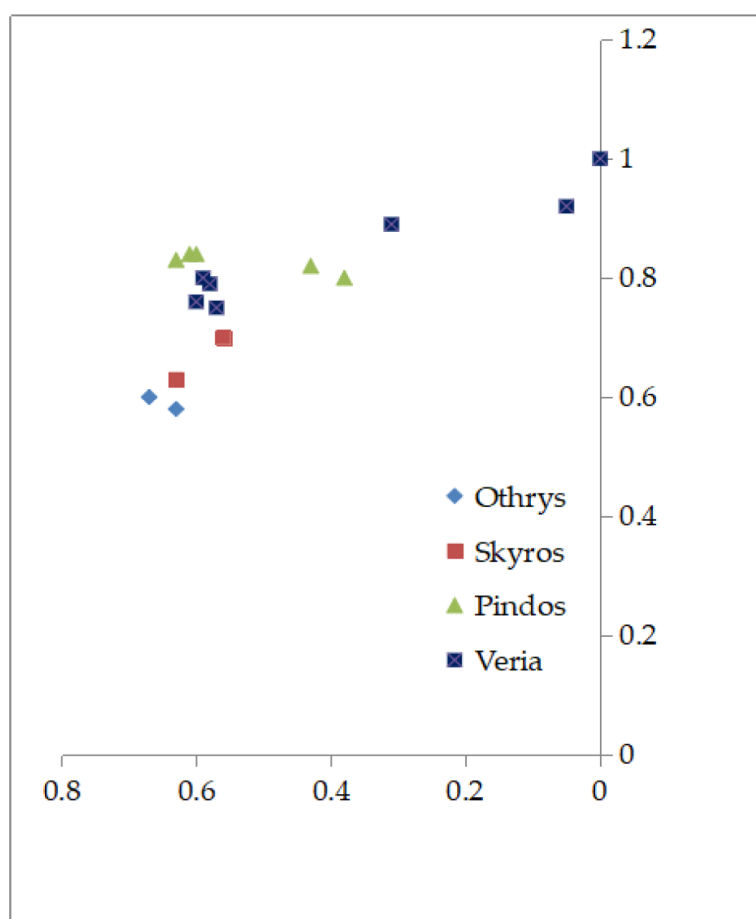


**Figure 7.** Plot of the Cr/(Cr + Al) ratio versus Mg/(Mg+Fe$^{2+}$) ratio for magnesio-chromite and chromite from the studied chromitites (Figures 3–6). Data are taken from Table 1 [39].

## 4.2. Geochemical Characteristics

The bulk rock analysis of carbon-bearing chromitites showed that the trace elements Ni, Co, Zn, and V, and platinum-group elements (Os, Ir, Ru, Rh, Pt, and Pd) (Table 2) fall in the range of previously

published data [41]. More specifically, the total PGE content of chromitites from the Othrys complex was lower than 100 ppb, as in the majority of the chromite deposits and occurrences associated with ophiolites [41]. Although the PGE content is generally low, there is a significant PGE enrichment in compatible (Os, Ir, Ru) or IPGE at Achladones in Skyros, Milia in Pindos, and Veria chromitites, while the Pd/Ir ratio, which is considered to reflect the fractionation degree of the parent magma [42] is relatively low in these chromitites. (Table 2). Selected trace elements, such as Ni, Co, V, and Zn, showed a small variation, and any relationship with the composition of the chromite (Cr# and Mg# ratios) was not obvious (Table 2).

**Table 2.** Major and trace element contents in carbon-bearing chromitites.

|  | Skyros | Othrys | Pindos | Veria | Detection Limit |
|---|---|---|---|---|---|
|  | Achladones | Eretria | Milia | Galaktos |  |
| ppb |  |  |  |  |  |
| Os | 140 | 24 | 150 | 7400 | 2 |
| Ir | 480 | 13 | 320 | 6020 | 2 |
| Ru | 1200 | 45 | 350 | 9700 | 5 |
| Rh | 160 | 3 | 82 | 310 | 1 |
| Pt | 280 | 8 | 150 | 760 | 5 |
| Pd | 39 | 1 | 8 | 750 | 1 |
| ΣPGE | 2300 | 94 | 1060 | 24,940 |  |
| Pd/Ir | 0.08 | 0.08 | 0.02 | 0.12 |  |
| Cr # | 0.61 | 0.56 | 0.82 | 0.79 |  |
| Mg # | 0.64 | 0.64 | 0.42 | 0.66 |  |
| ppm |  |  |  |  |  |
| Ni | 800 | 1350 | 1200 | 900 | 0.1 |
| Co | 250 | 230 | 350 | 200 | 0.2 |
| V | 890 | 1020 | 980 | 860 | 1 |
| Zn | 510 | 380 | 970 | 600 | 0.2 |

Symbols: Cr # = Cr/(Cr + Al); Mg # = Mg/(Mg + Fe$^{2+}$); PGE = platinum-group element.

## 5. Discussion

### 5.1. Abiotic Methane and Graphite

Abiotic $CH_4$ and graphite in serpentinized peridotites, chromitites, and magnetite ore were reported in several layered intrusions and ophiolite complexes [26,27]. Graphite is considered to be a reduced carbon species produced during the serpentinization of ultramafic rocks, with saturation in methane causing the precipitation of graphite, probably at low temperatures (500–300 °C) [23–28]. More specifically, most authors attributed the conditions of extremely low *fO$_2$* (reducing environment) during serpentinization not only to the widespread occurrence of native metals in serpentinites, but also to the occurrence of $H_2$ gas, released by reactions between Fe–Mg minerals, water, and carbonic acid during serpentinization, as shown below.

Fayalite + water → magnetite + aqueous silica + hydrogen,

$$3Fe_2SiO_4 + 2H_2O \rightarrow 2Fe_3O_4 + 3SiO_2 + 2H_2,$$
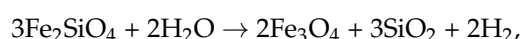
while the liberated silica reacts with Mg-olivine to form serpentine according to [43]
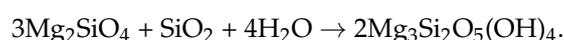
$$3Mg_2SiO_4 + SiO_2 + 4H_2O \rightarrow 2Mg_3Si_2O_5(OH)_4.$$

Methane ($CH_4$) can be produced via Fischer–Tropsch-type reactions (like the Sabatier reaction) between $CO_2$ (or other C compounds) and $H_2$ (from serpentinization) at low temperatures (typically <100 °C) [35,36], as shown below.

$$CO_2 + 4H_2 \rightarrow CH_4 + 2H_2O.$$
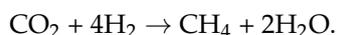
Regarding the source of carbon-bearing fluids, they could be magmatic, mantle-derived fluids [44], metamorphic decarbonation reactions, and devolatilization of organic matter (assimilation of rocks containing organic matter from the magmas). Due to the low solubility of carbon in silicate magmas, immiscibility results in the formation of carbon-rich magmas or fluids [45]. Thus, the mantle may provide $CO_2$ to the surface through degassing and magmatism, whereas carbon from sediments and altered oceanic crust can be recycled into the mantle through subduction [46,47].

*5.2. A Comparison between Graphite-Like Carbon in Chromitites of Greece and Other Chromitites and Peridotites*

Peridotites from the mantle sequence of ophiolites represent variously depleted residues of the primitive mantle after multi-stage partial melting events, melt extraction, and melt–rock interactions. The established wide range of compositional and geochemical heterogeneities in their bulk-rock compositions and mineral chemistries is inconsistent with their evolution through simple partial melting processes; they may be modified by subsequent progressive melting, depletion, and enrichment events at shallow mantle depths [9–11,15–18,48–50]. More specifically, the investigation of microdiamonds in chromitite and peridotite members of ophiolite complexes, such as in Tibet, Urals in Russia, Burma/Myanmar, Albanides in Albania, and Taurides in Turkey showed that they occur as cubo-octahedral polycrystalline or single crystals, and they contain fluid inclusions composed of water, carbonates, silicates, and hydrocarbons [15–18,48,49]. In general, diamonds found mostly in mineral concentrates from peridotites and chromitites of the mantle sequence of ophiolite complexes, along with ultra-high-pressure (UHP), super-reduced phases and continental crustal minerals, were interpreted as the result of their potential recycling into the ultra-deep mantle by continued subduction [15–17]. Also, it was suggested that the microdiamonds and highly reduced minerals in peridotites of the Dingqing ophiolite zone in Tibet are highly reduced minerals incorporated into chromian spinel grains near the Moho Transitional Zone (MTZ), but the mechanisms of their relatively rapid transportation from these depths to shallow mantle levels remain unclear [49].

Recently, the investigation of microdiamonds in situ, in chromite from ophiolite-type chromitites hosted in the Tehuitzingo serpentinite (southern Mexico), showed that they occur as fracture-filling inclusions, along with quartz, clinochlore, serpentine, and amorphous carbon, indicating a secondary origin during the shallow hydration of chromitite [11]. More specifically, these authors presented chromite chemical variations across the diamond-bearing healed fractures indicating formation during the retrograde evolution of chromitite at relatively low temperatures (520–670 °C) and concluded that diamonds precipitated as metastable phases at low pressure from reduced C–O–H fluids. In addition, the investigation of mineral concentrates from chromitite of the Mercedita (eastern Cuba) ophiolite complex deposit in the eastern Cuban ophiolitic complexes revealed the presence of oriented clinopyroxene lamellae and rutile in chromite, moissanite hosted in the altered matrix of the chromitite, graphite-like amorphous carbon, corundum and $SiO_2$ hosted in healed fractures in chromite grains, and native Cu and Fe–Mn alloys [11]. Although such an assemblage may correspond to UHP-SuR conditions, implying recycling of chromitite in the mantle or formation of the chromite grains at deep mantle depths, followed by emplacement at a shallow level in the mantle, the above authors documented that they formed during the serpentinization processes, and by transference of subducted crustal material to the mantle wedge via cold plumes. In addition, fluid inclusions in microdiamonds and their surrounding amorphous carbon may indicate that original fluids were rich in C, and that they contained Mn, Ni, Co, Si, Ti, Rare Earth Elements (REEs), and Cl, which occur abundantly in subducted oceanic slabs [50].

With respect to the presence C-bearing minerals in ophiolites, the application of carbon isotopic composition in fluid-deposited graphite is an efficient tool used to understand the origin of carbon (organic matter, mantle, or carbonates), both in the shallow and deep earth environments, helping constrain the fluid history and the mechanisms involved in graphite deposition [50]. Based on the carbon isotope ($\delta\,^{13}C$) data and nitrogen content for microdiamonds obtained from peridotites and chromitites of the Luobusa ophiolite in southern Tibet and chromitites from the Ray-Iz ophiolite in the Polar Urals of Russia [15,50], it was concluded that those microdiamonds incorporated into the chromitites and peridotites near the MTZ and were transported to the shallow mantle depths at very fast rates. Carbon stable isotopes on graphite from Alpine Corsica (France), formed during subduction metamorphism, showed $\delta^{13}C$ values up to $0.8 \pm 0.1\permil$, similar to that of the original calcite that composed the sediments, indicating that, under reducing and low-temperature conditions, there is a mechanism to retain carbon during its transport into the deeper earth [47]. Also, chemical differences ranging from $-20.5$ to $-27.8\permil$, in graphite from high-grade metapelitic rocks of the Anatectic Complex of Toledo (ACT), showed a biogenic origin [28]. The interaction of graphite with hydrothermal fluids did not modify isotopic compositions, even in the most transformed samples from mining sites, and differences in this case may reflect a different primary carbon source [28]. Furthermore, high-spatial-resolution carbon isotope analyses of natural graphite demonstrated isotopic heterogeneity within single graphite crystals in metamorphic rocks, attributed to the difference in diffusivity between $^{12}C$ and $^{13}C$ in the growth medium [51]. Although, in closed systems, carbon isotope systematics in graphite are mainly governed by Rayleigh precipitation and/or by changes in temperature, in open systems, in which carbon is episodically introduced along the fracture systems, the carbon isotope variations are more complex [52]. Thus, the isotopic composition cannot be used alone for the characterization of graphite and discrimination of its origin [53,54].

Geochemical and mineral chemistry characteristics for peridotites of Greece showed that the partial melting degree of primitive mantle and the hydrous nature of parent magma are major controlling factors of their composition [4,32,34–40,55]. In addition, the presence of diopside and andradite associated with serpentinized peridotites, phases indicative of a super-reducing environment, such as Fe–Ni–Cr alloys, awaruite, heazlewoodite, and graphite-like carbon (Figures 3–6), indicate that they were affected by post-magmatic processes. The occurrence of abundant spherulitic graphite, along with retrograde silicates in shear zones that served as fluid pathways through the chromitites, supports the role of C–O–H fluids in forming the graphite. Assuming that graphite-like carbon in chromitites of the Othrys complex, and probably in Skyros, Pindos, and Veria ores is the product of the methane saturation at shallow conditions probably at low temperatures (500–300 °C) [23–28], the presence of graphite-like carbon with chlorite healing cracks in the studied chromitites suggests that the graphite precipitation took place in an open system, allowing the introduction of carbon along the fracture systems, and suggests that it may have been facilitated by a strongly brittle (cataclastic) deformation. The widespread occurrence of metal alloys (Figure 3a) [32,35,40] and methane in microfractures and porous veins, and Ni–V–Co phosphides in chromitites from the Othrys ophiolite [24,56] suggesting an extremely low $fO_2$ (reducing environment) during serpentinization, are in agreement with the common occurrence of Fe–Ni–Cu-sulfide mineralization (pyrrhotite, chalcopyrite, and minor pentlandite), along with magnetite, at the peripheral parts of podiform chromite bodies [36]. Although the initial magmatic origin of those sulfides is not precluded, their texture characteristics showing a high transformation, and their geochemical features may indicate that the magmatic features were lost or metals were released from the host rocks by a low-level hydrothermal circulation process [36]. Such a reduction-induced sulfide saturation can drive the formation of magmatic sulfide deposits in the deep to shallow hydrothermal systems. In addition, the occurrence of sulfides and graphite in mantle-derived rocks [57], the Beni Bousera ultramafic massif (north Morocco) [58,59], and the Limassos area (Cyprus) [60] may reflect a mutual relationship between the origin of sulfur and carbon (deposition of sulfides and graphite). However, further research is required to delineate the carbon source(s) in chromitites.

### 5.3. Stability of Silicate Minerals, Graphite, and Alloys in Chromitites

Chromite was considered to remain unaltered, in terms of major or minor elements; however, a large database of analytical and experimental evidence showed that chromite may undergo significant alteration during post-magmatic processes, causing modification of chromite with the formation of homogeneous $Fe^{3+}$-rich rims (i.e., ferrian chromite) that often overgrow with $Fe^{2+}$-rich porous chromite [8–10,61]. Unusual magmatic ore assemblages consisting of Fe–Ni–Cu sulfides and graphite ± chromite occur within the ultramafic massif of the alpine Betic-Rif chain (south Spain and north Morocco) [58,59]. The development of $Fe^{2+}$-rich porous chromite is considered to be a prerequisite for the formation of ferrian chromite via diffusion of $Fe^{3+}$ into the pores of the previously formed porous chromite [8,18,62,63]. In addition, the decreasing w/r ratio may increase concentrations of calcium and hydroxide in the evolving aqueous phase, which becomes hyperalkaline and highly reducing [62].

The texture and mineral chemistry characteristics of the studied chromitites, showing graphite co-existing with $Fe^{2+}$-chromite along cracks within magnesio-chromite (Figures 6 and 7; Table 1), and the occurrence of $Fe^{3+}$-bearing garnet (dominantly andradite) as a matrix between chromite grains and fragments (Figure 6) [40] reflect changes of the redox conditions from reducing to oxidizing. Thus, the infiltrating C–O–H-rich fluids [24], the presence of hydrous silicates accompanied by graphite in the healed fractures of chromite, and the precipitation of garnets and hydroxyl silicates, during a subsequent stage confirm relatively low temperatures, as calculated in ophiolites [9–11]

### 5.4. The Role of the Ruthenium (PGE) Content

Chromitites associated with ophiolite complexes may contain considerable PGE content, including Ru, which is considered to be a powerful catalyst for $CO_2$ hydrogenation [25]. It was suggested that higher PGE contents (up to 100 ppb Ru) in chromitites compared to ophiolitic rocks in the Othrys complex are accompanied by the highest methane concentrations [24,25].

A detailed investigation of the PGE minerals [4,33,36–38] showed that minerals of the compatible elements Os, Ir, and Ru (or IPGE) in the studied chromitites are mostly oxides/hydroxides, in a matrix of silicates (with laurite existing only as small remnants), while any pure ruthenium was not identified. The recorded lack of any relationship between the presented PGE content in chromitites (covering a wide range from less than 100 ppb in Othrys to as high as 25 ppm ΣPGE in the Veria ores (Table 2)) and the abundance of graphite (Figures 3–6) may suggest that the methanogenesis and the subsequent precipitation of graphite are independent of the PGE content. Although the carbon dioxide methanogenesis reaction is thermodynamically favored, ($\Delta G_{298K}$ = −131 kJ·mol$^{-1}$), it requires a catalyst to activate the stable $CO_2$ molecule and reduce it to methane [47,63]. Pure ruthenium in contact with gas-phase $H_2$ and $CO_2$, which was used for experimental work [24], was absent in natural conditions, and further research is probably required to explore the mechanism and factors controlling the catalysis of the above reactions.

## 6. Conclusions

The first SEM/EDS data from polished and unpolished sections of chromitites from ophiolites of Greece showed the occurrence of graphite-like amorphous carbon associated with hydrous silicates (chlorite, serpentine), as inclusions in chromite, filling cracks within chromite, or as nodule-like graphite aggregates.

A characteristic feature of the chromitites is a strong brittle (cataclastic) texture and the presence of minerals indicative of super-reducing phases, such as graphite, Fe–Ni–Cr alloys, awaruite ($Ni_3Fe$), and heazlewoodite ($Ni_3S_2$).

The occurrence of graphite-like carbon in chromitites, in association with chlorite and/or serpentine, seems to be related to post-magmatic processes, probably during the sallow crustal brittle deformation.

The lack of any relationship between graphite abundance and PGE content of chromitites may reflect that a special oxidation stage of ruthenium is required to catalyze the methanogenesis reaction from $CO_2$.

## References

1. Economou, M.; Dimou, E.; Economou, G.; Migiros, G.; Vacondios, I.; Grivas, E.; Rassios, A.; Dabitzias, S. *Chromite Deposits of Greece: Athens*; Theophrastus Publications: Athens, Greece, 1986; pp. 129–159.
2. Melcher, F.; Grum, W.; Simon, G.; Thalhammer, T.V.; Stumpfl, E. Petrogenesis of the ophiolitic giant chromite deposit of Kempirsai, Kazakhstan: A study of solid and fluid inclusions in chromite. *J. Petrol.* **1997**, *10*, 1419–1458. [CrossRef]
3. Proenza, J.A.; Gervilla, F.; Melgarejo, J.C.; Bodinier, J.L. Al- and Cr-rich chromitites from the Mayarí-Baracoa ophiolitic belt (eastern Cuba); consequence of interaction between volatile-rich melts and peridotites in suprasubduction mantle. *Econ. Geol.* **1999**, *94*, 547–566. [CrossRef]
4. Garuti, G.; Zaccarini, F.; Economou-Eliopoulos, M. Paragenesis and composition of laurite from the chromitites of Othrys (Greece): Implications for Os-Ru fractionation in ophiolitic upper mantle of the Balkan Peninsula. *Miner. Depos.* **1999**, *34*, 312–319. [CrossRef]
5. Beccaluva, L.; Coltorti, M.; Saccani, E.; Siena, F. Magma generation and crustal accretion as evidenced by supra-subduction ophiolites of the Albanide-Hellenide Sub Pelagonian zone. *Island Arc* **2005**, *14*, 551–563. [CrossRef]
6. Rassios, A.; Konstantopoulou, G. Emplacement tectonism and the position of chrome ores in the Mega Isoma peridotites, SW Othris, Greece. *Bull. Geol. Soc. Greece* **1993**, *28*, 463–474.
7. Rassios, A.; Dilek, Y. Rotational deformation in the Jurassic Mesohellenic Ophiolites, Greece, and its tectonic significance. *Lithos* **2009**, *108*, 207–223. [CrossRef]
8. Gervilla, F.; Padrón-Navarta, J.A.; Kerestedjian, T.; Sergeeva, I.; González-Jiménez, J.M.; Fanlo, I. Formation of ferrian chromite in podiform chromitites from the Golyamo Kamenyane serpentine, Eastern Rhodopes, SE Bulgaria: A two-stage process. *Contr. Mineral. Petrol.* **2012**. [CrossRef]
9. Colás, V.; González-Jiménez, J.M.; Griffin, W.L.; Fanlo, I.; Gervilla, F.; O'Reilly, S.Y.; Pearson, N.J.; Kerestedjian, T.; Proenza, J.A. Fingerprints of metamorphism in chromite: New insights from minor and trace elements. *Chem. Geol.* **2014**, *389*, 137–152. [CrossRef]
10. González-Jiménez, J.M.; Locmelis, M.; Belousova, E.; Griffin, W.L.; Gervilla, F.; Kerestedjian, T.N.; Pearson, N.J.; Sergeeva, I. Genesis and tectonic implications of podiform chromitites in the metamorphosed Ultramafic Massif of Dobromirtsi (Bulgaria). *Gondwana Res.* **2015**, *27*, 555–574. [CrossRef]
11. Pujol-Solà, N.; Proenza, I.A.; Garcia-Casco, A.; González-Jiméne, J.M.; Andreazini, A.; Melgarejo, J.C.; Gervilla, F. An Alternative Scenario on the Origin of Ultra-High Pressure (UHP) and Super-Reduced (SuR) Minerals in Ophiolitic Chromitites: A Case Study from the Mercedita Deposit (Eastern Cuba). *Minerals* **2018**, *8*, 433. [CrossRef]
12. Arai, S. Conversion of low-pressure chromitites to ultrahig-pressure chromitites by deep recycling: A good inference. *Earth Planet. Sci. Lett.* **2013**, *379*, 81–87. [CrossRef]
13. Ballhaus, C.G.; Stumpfl, E.F. Occurrence and petrological significance of graphite in the Upper Critical Zone, western Bushveld Complex, South Africa. *Earth Plant Sci. Lett.* **1985**, *74*, 58–68. [CrossRef]
14. Zhou, M.F.; Robinson, P.T.; Su, B.X.; Gao, J.F.; Li, J.W.; Yang, J.S.; Malpas, J. Compositions of chromite, associated minerals, and parental magmas of podiform chromite deposits: The role of slab contamination of asthenospheric melts in suprasubduction zone environments. *Gondwana Res.* **2014**, *26*, 262–283. [CrossRef]

15. Yang, J.S.; Meng, F.; Xu, S.; Robinson, P.T.; Dilek, Y.; Makeyev, A.B.; Wirth, R.; Wiedenbeck, M.; Cliff, J. Diamonds, native elements and metal alloys from chromitite of the Ray-Iz ophiolite of the Polar Urals. *Gondwana Res.* **2015**, *27*, 459–485. [CrossRef]

16. Robinson, P.T.; Trumbull, R.B.; Schmitt, A.; Yang, J.S.; Li, J.W.; Zhou, M.F.; Erzinger, J.; Dare, S.; Xiong, F. The origin and significance of crustal minerals in ophiolitic chromitites and peridotites. *Gondwana Res.* **2015**, *27*, 486–506. [CrossRef]

17. Xiong, F.; Yang, J.; Dilek, Y.; Xu, X.; Zhang, Z. Origin and significance of diamonds and other exotic minerals in the Dingqing ophiolite peridotites, eastern Bangong-Nujiang suture zone, Tibet. *Lithosphere* **2017**, *10*, 142–155. [CrossRef]

18. Farré-de-Pablo, J.; Proenza, I.A.; González-Jiménez, J.M.; Garcia-Casco, A.; Colás, V.; Roqué-Rosse, L.; Camprubí, A.; Sánchez-Navas, A. A shallow origin for diamonds in ophiolitic chromitites. *Geology* **2018**. [CrossRef]

19. Frost, B.R. On the stability of sulfides, oxides and native metals in serpentinites. *J. Petrol.* **1985**, *26*, 31–63. [CrossRef]

20. McKee, D.W. Carbon and graphite science. *Ann. Rev. Mater. Sci.* **1973**, *3*, 195–231. [CrossRef]

21. Seewald, J.S.; Zolotov, M.Y.; McCollom, T. Experimental investigation of single carbon compounds under hydrothermal conditions. *Geochim. Cosmochim. Acta* **2006**, *70*, 446–460. [CrossRef]

22. Tsikouras, B.; Etiope, G.; Ifandi, E.; Kordella, S.; Papatheodorou, G.; Hatzipanagiotou, K. Methane flux and origin in the Othrys ophiolite hyperalkaline springs, Greece. *Chem. Geol.* **2013**, *347*, 161–174.

23. Brovarone, A.B.; Martinez, I.; Elmaleh, A.; Compagnoni, R.; Chaduteau, C.; Ferraris, C.; Esteve, I.; Brovarone, A.B.; Martinez, I.; Elmaleh, A.; et al. Massive production of abiotic methane during subduction evidenced in metamorphosed ophicarbonates from the Italian Alps. *Nat. Commun.* **2017**, *E18*, 14134. [CrossRef] [PubMed]

24. Etiope, G.; Ifandi, E.; Nazzari, M.; Procesi, M.; Tsikouras, B.; Ventura, G.; Steele, A.; Tardini, R.; Szatmari, P. Widespread abiotic methane in chromitites. *Sci. Rep.* **2018**, *8*, 8728. [CrossRef] [PubMed]

25. Etiope, G.; Ionescu, A. Low-temperature catalytic $CO_2$ hydrogenation with geological quantities of ruthenium: A possible abiotic CH4 source in chromitite-rich serpentinized rocks. *Geofluids* **2015**, *15*, 438–452. [CrossRef]

26. Stumpfl, E.F.; Rucklidge, J.C. The platiniferous dunite pipes of the eastern Bushveld Complex. *Econ. Geol.* **1982**, *77*, 1419–1431. [CrossRef]

27. Volborth, A.A.; Housley, R.M. A preliminary description of complex graphite, sulphide, arsenide, and platinum-group element mineralization in a pegmatoid pyroxenite of the Stillwater Complex, Montana, USA. *TMPM* **1984**, *33*, 213–230. [CrossRef]

28. Martín-Méndez, I.; Boixereu, E.; Villaseca, C. Mineralogical and isotopic characterization of graphite deposits from the Anatectic Complex of Toledo, central Spain. *Min. Depos.* **2016**, *551*, 575. [CrossRef]

29. Spray, J.G.; Bébien, J.; Rex, D.C.; Roddick, J.C. Age constraints on the igneous and metamorphic evolution of the Hellenic-Dinaric ophiolites. *Geol. Soc. Lond. Spec. Publ.* **1984**, *17*, 619–627. [CrossRef]

30. Hirsch, P.; Kassens, S.; Puttmann, P.; Reimer, L. Contamination in a Scanning Electron Microscope and the Influence of Specimen Cooling. *Scanning* **1994**, *16*, 101–110. [CrossRef]

31. Postek, M.T. An approach to the reduction of hydrocarbon contamination in the scanning electron microscope. *Scanning* **1996**, *18*, 269–274. [CrossRef]

32. Kapsiotis, A.; Rassios, A.; Antonelou, A.; Tzamos, E. Genesis and Multi-episodic Alteration of Zircon-bearing Chromitites from Ayios Stefanos, Othris Massif, Greece: Assessment of an Unconventional Hypothesis on the Origin of Zircon in Ophiolitic Chromitites. *Minerals* **2016**, *6*, 124. [CrossRef]

33. Moudrakis, D. Introduction to the geology of Macedonia and Trace: Aspects of the geotectonic evolution of the Hellenides. *Bull. Geol. Soc. Greece* **1992**, *30*, 31–46.

34. Economou-Eliopoulos, M. On the origin of the PGE-enrichment in chromitites associated with ophiolite complexes: The case of Skyros island, Greece. In *9th SGA Meeting*; Andrew, C.J., Borg, G., Eds.; Digging Deeper: Dublin, Ireland, 2007; pp. 1611–1614.

35. Tarkian, M.; Eliopoulos, D.; Economou-Eliopoulos, M. Platinum-group minerals and tetraauricuprite in ophiolitic rocks of the Skyros Island, Greece. *Mineral. Petrol.* **1992**, *47*, 55–56. [CrossRef]

36. Economou, M.; Naldrett, A.J. Sulfides associated with podiform bodies of chromite at Tsangli, Eretria, Greece. *Mineral. Depos.* **1984**, *19*, 289–297. [CrossRef]

37. Economou-Eliopoulos, M.; Vacondios, I. Geochemistry of chromitites and host rocks from the Pindos ophiolite complex, northwestern Greece. *Chem. Geol.* **1995**, *122*, 99–108. [CrossRef]

38. Prichard, H.; Economou-Eliopoulos, M.; Fisher, P.C. Contrasting Platinum-group mineral assemblages from two different podiform chromitite localities in the Pindos ophiolite complex, Greece. *Can. Mineral.* **2008**, *46*, 329–341. [CrossRef]

39. Kapsiotis, A.; Grammatikopoulos, T.; Tsikouras, B.; Hatzipanagiotou, K.; Zaccarini, F.; Garuti, G. Chromian spinel composition and Platinum-group element mineralogy of chromitites from the Milia area, Pindos ophiolite complex, Greece. *Can. Mineral.* **2009**, *47*, 1037–1056. [CrossRef]

40. Tsoupas, G.; Economou-Eliopoulos, M. High PGE contents and extremely abundant PGE-minerals hosted in chromitites from the Veria ophiolite complex, northern Greece. *Ore Geol. Rev.* **2008**, *33*, 3–19. [CrossRef]

41. Economou-Eliopoulos, M.; Eliopoulos, D.G.; Tsoupas, G. On the diversity of the PGE content in chromitites hosted in ophiolites and in porphyry-Cu systems: Controlling factors. *Ore Geol. Rev.* **2017**, *88*, 156–173. [CrossRef]

42. Barnes, S.-L.; Naldrett, A.J.; Gorton, M.P. The origin of the fractionation of the platinum-group elements in terrestrial magmas. *Chem. Geol.* **1985**, *53*, 203–323. [CrossRef]

43. Barnes, I.; O'Neil, J.R. The relationships between fluids in some fresh alpine-type ultramafics and possible serpentinization, Western United States. *Geol. Soc. Bull.* **1969**, *80*, 1947–1960. [CrossRef]

44. Kvasnitsa, V.N.; Yatsenko, V.G.; Jaszczok, J.A. Disclinations in unusual graphite crystals from anorthosites of Ukraine. *Can. Mineral.* **1999**, *35*, 951–960.

45. Rodas, M.; Luque, F.J.; Barrenechea, J.F.; Fernandez-Caliani, J.C.; Miras, A.; Fernandez-Rodriguez, C. Graphite occurrences in the low-pressure/hightemperature metamorphic belt of the Sierra de Aracena (southern Iberian Massif). *Mineral. Mag.* **1999**, *64*, 801–814. [CrossRef]

46. Coltice, N.; Simon, L.; Lecuyer, C. Carbon isotope cycle and mantle structure. *Geophys. Res. Lett.* **2004**, *31*, L05603. [CrossRef]

47. Gálvez, M.E.; Beyssac, O.; Martinez, I.; Benzerara, K.; Chaduteau, C.; Malvosin, B.; Malavieille, J. Graphite formation by carbonate reduction during subduction. *Nat. Geosci.* **2013**, *6*, 473–477. [CrossRef]

48. Lian, D.-Y.; Yang, J.-S.; Dilek, Y.; Wu, W.W.; Zhang, Z.-M.; Xiong, F.; Liu, F.; Zhou, W. Deep mantle origin and ultra-reducing conditions in podiform chromitite: Diamond, mois sanite, and other unusual minerals in podiform chromitites from the Pozanti-Karsanti ophiolite, southern Turkey. *Am. Mineral.* **2017**, *102*, 1101–1113. [CrossRef]

49. Dilek, Y.; Yang, J. Ophiolites, diamonds, and ultrahigh-pressure minerals: New discoveries and concepts on upper mantle petrogenesis. *Lithosphere* **2018**, *10*, 3–13. [CrossRef]

50. Xu, X.-Z.; Cartigny, P.; Yang, J.-S.; Dilek, Y.; Xiong, F.; Guo, G. Fourier trans-form infrared spectroscopy data and carbon isotope characteristics of the ophiolite-hosted diamonds from the Luobusa ophiolite, Tibet, and Ray-Iz ophiolite, Polar Urals. *Lithosphere* **2018**, *10*, 156–169. [CrossRef]

51. Satish-Kumar, M.; So, H.; Yoshino, T.; Kato, M.; Hiroi, Y. Experimental determination of carbon isotope fractionation between iron carbide melt and carbon: $^{12}$C-enriched carbon in the Earth's core? *Earth Planet. Sci. Lett.* **2011**, *310*, 340–348. [CrossRef]

52. Luque, F.J.; Crespo-Feo, E.; Barrenechea, J.F.; Ortega, L. Carbon isotopes of graphite: Implications on fluid history. *Geosci. Front.* **2013**, *3*, 197–207. [CrossRef]

53. Van Zuilen, M.A.; Lepland, A.; Arrhenius, G. Reassessing the evidence for the earliest traces of life. *Nature* **2002**, *418*, 627–630. [CrossRef] [PubMed]

54. Lopez-Garcia, P.; Moreira, D.; Douzery, E.; Forterre, P.; Van Zuilen, M.; Claeys, P.; Prieur, D. Ancient fossil record and early evolution (ca. 3.8 to 0.5 Ga). *Earth Moon Planets* **2002**, *98*, 247–290. [CrossRef]

55. Kapsiotis, A.; Economou-Eliopoulos, M.; Zhenga, H.; Sud, B.X.; Lenaz, D.; Jing, J.J.; Antoneloug, A.; Velicogna, M.; Xia, B. Refractory chromitites recovered from the Eretria mine, East Othris massif (Greece): Implications for metallogeny and deformation of chromitites within the lithospheric mantle portion of a forearc-type ophiolite. *Chemie der Erde* **2019**, in press.

56. Ifandi, E.; Zaccarini, Z.; Tsikouras, B.; Grammatikopoulos, T.; Garuti, G.; Karipi, S. First occurrences of Ni-V-Co phosphides in chromitite from the Agios Stefanos Mine, Othrys Ophiolite, Greece. *Ofioliti* **2018**, *43*, 131–145.

57. Tomkins, A.G.; Rebryna, K.C.; Weinberg, R.F.; Schaefer, B.F. Magmatic sulfide formation by reduction of oxidized arc basalt. *J. Petrol.* **2012**, *53*, 1537–1567. [CrossRef]

58. Gervilla, F.; Essaifi, A.; Wafik, A. Mineralogical and geochemical features of the alteration processes of magmatic ores in the Beni Bousera ultramafic massif (north Morocco). *J. Afr. Earth Sci.* **2017**, *132*, 47–63.

59. Gervilla, F.; Leblanc, M.; Torres-Ruiz, J.; Fenoll Hach-Ali, P. Immiscibility between arsenide and sulfide melts: A mechanism for the concentration of noble metals. *Can. Mineral.* **1996**, *34*, 485–502.

60. Panayiotou, A. *Cu-Ni-Co-Fe Sulphide Mineralization, Limassol Forest, Cyprus*; Panayiotou, A., Ed.; International Ophiolite Symposium: Nicosia, Cyprus, 1980; pp. 102–116.

61. Zaccarini, F.; Proenza, A.J.; Ortega-Gutierrez, F.; Garuti, G. Platinum group minerals in ophiolitic chromitites from Tehuitzingo (Acatlan complex, southern Mexico): Implications for post-magmatic modification. *Mineral. Petrol.* **2005**, *84*, 147–168. [CrossRef]

62. Palandri, J.L.; Reed, M.H. Geochemical models of metasomatism in ultramafic systems: Serpentinization, rodingitization, and sea floor carbonate chimney precipitation. *Geochim. Cosmochim. Acta* **2004**, *68*, 1115–1133. [CrossRef]

63. Holloway, J.R. Graphite-$CH_4$-$H_2O$-$CO_2$ equilibrium at low-grade metamorphic conditions. *Geology* **1984**, *12*, 455–458. [CrossRef]